

RESEARCH ARTICLE | JANUARY 03 2025

Phase stability and transition behaviors of $(\text{BiIn}_{1-x})_2\text{Se}_3$ alloy



Huachun Wang ; Xuefen Cai ; Wei Li ; Bin Wang ; Igor Evangelista ; Anderson Janotti



Appl. Phys. Lett. 126, 012106 (2025)

<https://doi.org/10.1063/5.0243242>

CHORUS



View
Online



Export
Citation

Articles You May Be Interested In

Interlayer-glide-driven isosymmetric phase transition in compressed In_2Se_3

Appl. Phys. Lett. (May 2014)

Photoluminescence of bulk α - In_2Se_3 crystals irradiated by high-energy electrons

Appl. Phys. Lett. (December 2023)

Molecular beam epitaxy synthesis of In_2Se_3 films

J. Vac. Sci. Technol. A (April 2024)



Applied Physics Letters

Special Topics Open
for Submissions

[Learn More](#)

Phase stability and transition behaviors of $(\text{Bi}_x\text{In}_{1-x})_2\text{Se}_3$ alloy

Cite as: Appl. Phys. Lett. **126**, 012106 (2025); doi: [10.1063/5.0243242](https://doi.org/10.1063/5.0243242)

Submitted: 9 October 2024 · Accepted: 26 December 2024 ·

Published Online: 3 January 2025



View Online



Export Citation



CrossMark

Huachun Wang,¹ Xuefen Cai,^{2,a)} Wei Li,³ Bin Wang,² Igor Evangelista,³ and Anderson Janotti^{3,a)}

AFFILIATIONS

¹School of Integrated Circuits, Shenzhen Campus of Sun Yat-sen University, Shenzhen 518107, China²State Key Laboratory of Radio Frequency Heterogeneous Integration (Shenzhen University), College of Physics and Optoelectronic Engineering, Shenzhen University, Shenzhen 518060, China³Department of Materials Science and Engineering, University of Delaware, Newark, Delaware 19716, USA^{a)}Authors to whom correspondence should be addressed: caixuefen@szu.edu.cn and janotti@udel.edu

ABSTRACT

The Bi_2Se_3 – In_2Se_3 layered system has garnered significant attention and extensive research due to its versatile properties, yet its structural properties and phase stability remain elusive. Here, using first-principles calculations with van der Waals interactions, we systematically study the phase stability and transition behavior of $(\text{Bi}_x\text{In}_{1-x})_2\text{Se}_3$ alloys. Our results reveal a contrasting stability profile between Bi_2Se_3 and In_2Se_3 , with the former exhibiting a distinct preference for the β phase over the α phase, while the latter shows similar stabilities in both phases, thus partially addressing previously reported ground-state inconsistencies. Exploring composition–structure relationships, we demonstrate that Bi incorporation in low concentrations stabilizes the β phase, consistent with early experimental observations. Further analysis based on the cation orbital properties indicates that the preference of Bi for octahedral sites over tetrahedral ones drives the small critical composition for the $\alpha \rightarrow \beta$ phase transition. This work enhances our understanding of phase stability in $(\text{Bi}_x\text{In}_{1-x})_2\text{Se}_3$ alloys, providing insights for future design of monophasic materials and advanced applications.

Published under an exclusive license by AIP Publishing. <https://doi.org/10.1063/5.0243242>

Two-dimensional (2D) layered chalcogenides, such as GaSe, MoS_2 , TiSe_2 , In_2Se_3 , Bi_2Se_3 , and Bi_2Te_3 , are gaining significant attention because of their rich and unique physical properties, with potential applications in diverse electronics and optoelectronics. Among these, the III–VI chalcogenide In_2Se_3 , being a compound equipped with promising photo-,^{1–4} thermo-,^{5–8} and ferroelectric properties,^{9–12} has long been one of the most extensively studied 2D materials. In_2Se_3 is polymorphic, crystallizing in layered α , β , δ , and κ phases, and the defect wurtzite γ phase at ambient pressure. The α and β phases, with space groups $R\bar{3}m$ and $R\bar{3}m$, respectively, are the two major layered polymorphs of In_2Se_3 . Note that the terminology, phase stability, and transformation conditions of In_2Se_3 reported in the literature are not always consistent, and even the ground-state phase is still debated.^{5,9,13} Each polytype corresponds to different electronic and optical properties. The polymorphism of In_2Se_3 makes it a promising candidate for phase-change materials in data storage applications. However, the facile phase transition in In_2Se_3 may pose challenges for optoelectronic devices like photodetectors. Therefore, understanding and effectively controlling the phase transition in In_2Se_3 is crucial for its practical applications.

β - Bi_2Se_3 (with space group of $R\bar{3}m$) is another notable chalcogenide, well-known as a topological insulator (TI). TIs represent a quantum matter state characterized by insulating bulk and gapless, metallic surface states. Due to the unique properties and hexagonal structural compatibility between layered In_2Se_3 and Bi_2Se_3 , the Bi_2Se_3 – In_2Se_3 system in random alloy^{14–16} or superlattice structure^{17–19} has recently drawn great attention. Notably, $(\text{Bi}_x\text{In}_{1-x})_2\text{Se}_3$ alloys have been experimentally demonstrated to exhibit broad tunability from a topological metal to a truly insulating state.¹⁴ While extensive investigations have focused on the topological properties of alloys with high Bi concentration, scant attention has been given to the structural properties and phase stability of low Bi content $(\text{Bi}_x\text{In}_{1-x})_2\text{Se}_3$ alloys. Only a few prior experimental studies indicate that the dilute substitution of In by Bi stabilizes the system in $R\bar{3}m$ phase akin to the pure β - Bi_2Se_3 structure.^{20,21} Therefore, to deepen the understanding of the phase stability of the Bi_2Se_3 – In_2Se_3 system and promote further alternative applications, a systematic investigation is necessary.

In this work, using first-principles calculations, we first study and compare the stability of In_2Se_3 and Bi_2Se_3 in both α and β phases. To account for the van der Waals (vdW) interactions in layered In_2Se_3

and Bi_2Se_3 , we employ two sets of functionals: the popular Heyd-Scuseria-Ernzerhof (HSE06) screened hybrid density functional²² with the semi-empirical DFT-D3 vdW corrections of Grimme^{23,24} (HSE06+D3), and the recently developed strongly constrained and appropriately normed (SCAN) functional with the revised Vydrov-van Voorhis nonlocal correlation (SCAN+rVV10),²⁵ known for providing reliable interlayer binding energies and spacings for various layered materials. The results show consistently that for In_2Se_3 , the stabilities of the α and β phases are very close, partially explaining the inconsistency of the various reports discussing the ground-state structure. For Bi_2Se_3 , however, the β phase is significantly more stable than the α phase. We then explore the composition-structure relationships and construct the temperature-composition phase diagram for random $(\text{Bi}_x\text{In}_{1-x})_2\text{Se}_3$ alloys across the entire range of Bi compositions. Our findings align with reported experimental results,^{20,21} demonstrating that the introduction of Bi into In_2Se_3 progressively stabilizes the β phase. The calculated critical composition (x_c) for the $\alpha \rightarrow \beta$ transition is only $\sim 3\%$ ($\sim 10\%$) within HSE06+D3 (SCAN+rVV10). We analyze the mechanism leading to this small x_c by examining the nature of the cation orbitals. This work elucidates the phase stability in $(\text{Bi}_x\text{In}_{1-x})_2\text{Se}_3$ systems and offers fundamental insights that can guide the synthesis of monophasic materials, which are valuable for designing advanced electronics and optoelectronics.

Our first-principles calculations are conducted using the projector augmented wave (PAW) method²⁶ and density functional theory (DFT) as implemented in the Vienna *Ab initio* Simulation Package (VASP).²⁷ We have carried out calculations at two different levels, including HSE06+D3 and SCAN+rVV10. For HSE06+D3, the Hartree-Fock exchange mixing parameter α is set to 25%. We set the plane wave cutoff energy to 320 eV and sample the Brillouin zone using a Γ -centered $6 \times 6 \times 6$ Monkhorst-Pack (MP) k mesh for the primitive cell of In_2Se_3 and Bi_2Se_3 . As shown in Table I, the calculated lattice parameters for conventional unit cells (with $\alpha = \beta = 90^\circ$, $\gamma = 120^\circ$) of α - and β - In_2Se_3 and β - Bi_2Se_3 , using HSE06+D3 and SCAN+rVV10 functionals agree well with the available experimental

TABLE I. Calculated lattice parameters (a and c) and formation enthalpy ΔH_f for In_2Se_3 and Bi_2Se_3 in both α ($R3m$) and β ($R\bar{3}m$) phases using HSE06+D3 and SCAN+rVV10 functionals. Available experimental values are also listed.

		a (Å)	c (Å)	ΔH_f (eV)
α - In_2Se_3	HSE06+D3	4.01	28.64	-3.291
	SCAN+rVV10	4.06	28.59	-3.163
	Expt. ^{13,28}	4.00	28.80	-3.296
β - In_2Se_3	HSE06+D3	3.92	27.71	-3.217
	SCAN+rVV10	3.97	27.67	-3.064
	Expt. ²⁹	4.00	28.33	...
α - Bi_2Se_3	HSE06+D3	4.18	29.36	-1.099
	SCAN+rVV10	4.23	29.59	-0.836
	Expt.
β - Bi_2Se_3	HSE06+D3	4.09	28.86	-2.144
	SCAN+rVV10	4.13	28.89	-1.666
	Expt. ^{30,31}	4.14	28.64	-1.6

data.^{13,28-31} The formation enthalpies ΔH_f of In_2Se_3 and Bi_2Se_3 are also presented in Table I.

To simulate random $(\text{Bi}_x\text{In}_{1-x})_2\text{Se}_3$ alloys, we construct special quasi-random structures (SQS)³² based on a 240-atom supercell, where 0, 1, 3, 6, 12, 24, 48, 72, and 96 In atoms are replaced by Bi, corresponding to Bi compositions x of 0% (In_2Se_3), 1.04%, 3.125%, 6.25%, 12.5%, 25%, 50%, 75%, and 100% (Bi_2Se_3). Both the α and β phases are studied. The atomic positions of the SQS cells are fully relaxed using a Γ -centered $2 \times 2 \times 1$ Monkhorst-Pack k mesh, with convergence criteria set to 10^{-5} eV in energy and 0.05 eV/Å in Hellmann-Feynman force on each atom.

Figure 1 illustrates the conventional unit cells of $M_2\text{Se}_3$ ($M = \text{In}, \text{Bi}$) in both α and β phases, belonging to the $R3m$ and $R\bar{3}m$ space groups, respectively. The lattice of the α (β) phase can be seen as a hexagonal 2D layered structure composed of a sequence of quintuple layers (QL) arranged as Se- M -Se- M -Se. Within a QL, the chemical bonds between the cation and anion atoms are characterized as covalent-ionic, while neighboring QLs are bound by weak van der Waals (vdW) interactions. The α and β phases exhibit distinct local atomic environments and stacking arrangements of the atomic layers within the QL. In the α phase, the stacking sequence of the atomic layers follows an ABBCA pattern. There are two types of cation environments with varying coordination to anion atoms: one with tetrahedral (Tet.) and the other with octahedral (Oct.) coordination geometry. Conversely, the β phase displays a stacking sequence of ABCAB for the QL atomic layers, featuring only one type of cation site with octahedral coordination. As shown in Fig. 1, the α and β phases can be simplified as Tet-Oct and Oct-Oct structures, respectively.

The formation enthalpy ΔH_f of $M_2\text{Se}_3$ (with M being In or Bi) is given by

$$\Delta H_f = E(M_2\text{Se}_3) - 2E(M) - 3E(\text{Se}). \quad (1)$$

Here, $E(M_2\text{Se}_3)$ represents the total energy per formula unit (containing two cations) of $M_2\text{Se}_3$ in either the α or β phase, while $E(M)$ and $E(\text{Se})$ are the total energies per atom of bulk M and Se, respectively.

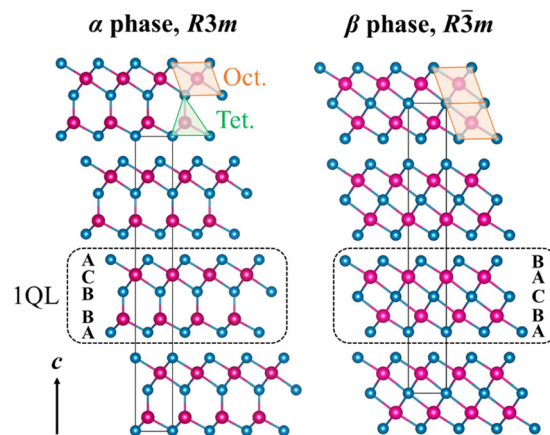


FIG. 1. Conventional unit cells of α - and β - $M_2\text{Se}_3$ ($M = \text{In}, \text{Bi}$). The purple-red spheres denote the cation M atoms and blue-colored spheres denote the anion Se atoms. The black dashed boxes represent one quintuple layer (QL). The stacking sequences within each QL for the both phases are shown. The $M\text{Se}_6$ octahedron (Oct) and $M\text{Se}_4$ tetrahedron (Tet) are highlighted in the upper part of the figure.

The calculated formation enthalpies for both In_2Se_3 and Bi_2Se_3 in both α and β phases using HSE06+D3 and SCAN+rVV10 functionals are listed in Table I, along with available experimental data. The ground-state phase of In_2Se_3 is the α phase, while that of Bi_2Se_3 is the β phase. For clarity, as depicted in Fig. 2(a), we illustrate the energy difference between the α and β phases of In_2Se_3 and Bi_2Se_3 calculated using HSE06+D3 and SCAN+rVV10. It is observed that the energy difference between α - and β - In_2Se_3 (purple-red bar) is considerably smaller compared to that of Bi_2Se_3 (blue bar) using both functionals, with a more pronounced difference within HSE06+D3 compared to SCAN+rVV10. To evaluate the influence of SOC on the total energy of Bi_2Se_3 , we incorporate SOC effects into the HSE06+D3 calculations. The inclusion of SOC results in an energy difference (between α and β) of 0.981 eV for Bi_2Se_3 , as indicated by the white dashed line in Fig. 2(a), compared to 1.045 eV within HSE06+D3 without SOC. Considering this relatively minor quantitative distinction and the heavy computational burden of SOC calculations, we do not include SOC effects in the study of $(\text{Bi}_x\text{In}_{1-x})_2\text{Se}_3$ alloys.

To access the stability of $(\text{Bi}_x\text{In}_{1-x})_2\text{Se}_3$ alloys, we examine the mixing enthalpy (ΔH) of α - and β -alloys with varying Bi concentrations x , expressed as follows:

$$\Delta H(x) = E[(\text{Bi}_x\text{In}_{1-x})_2\text{Se}_3] - (1-x)E(\text{In}_2\text{Se}_3) - xE(\text{Bi}_2\text{Se}_3), \quad (2)$$

where $E[(\text{Bi}_x\text{In}_{1-x})_2\text{Se}_3]$ is the total energy of the SQS supercell of $(\text{Bi}_x\text{In}_{1-x})_2\text{Se}_3$ alloy. $E(\text{In}_2\text{Se}_3)$ and $E(\text{Bi}_2\text{Se}_3)$ represent the total energies of α - In_2Se_3 and β - Bi_2Se_3 supercells, respectively. Accordingly, the enthalpies of pure α - In_2Se_3 and β - Bi_2Se_3 are both set to zero. The results obtained for α - and β - $(\text{Bi}_x\text{In}_{1-x})_2\text{Se}_3$ alloys using HSE06+D3 and SCAN+rVV10 functionals are shown in Figs. 2(b)–2(e). The two functionals exhibit a comparable trend in the evolution of the mixing enthalpy for $(\text{Bi}_x\text{In}_{1-x})_2\text{Se}_3$ alloys. It is observed that the alloys remain energetically in the α phase within a dilute Bi composition range. However, as the Bi concentration increases and surpasses a critical value (x_c), the mixing enthalpy of β - $(\text{Bi}_x\text{In}_{1-x})_2\text{Se}_3$ alloys becomes lower than that of α -alloys, indicating a shift in the stable phase of alloys to β for $x > x_c$. The critical value x_c is $\sim 3\%$ using HSE06+D3,

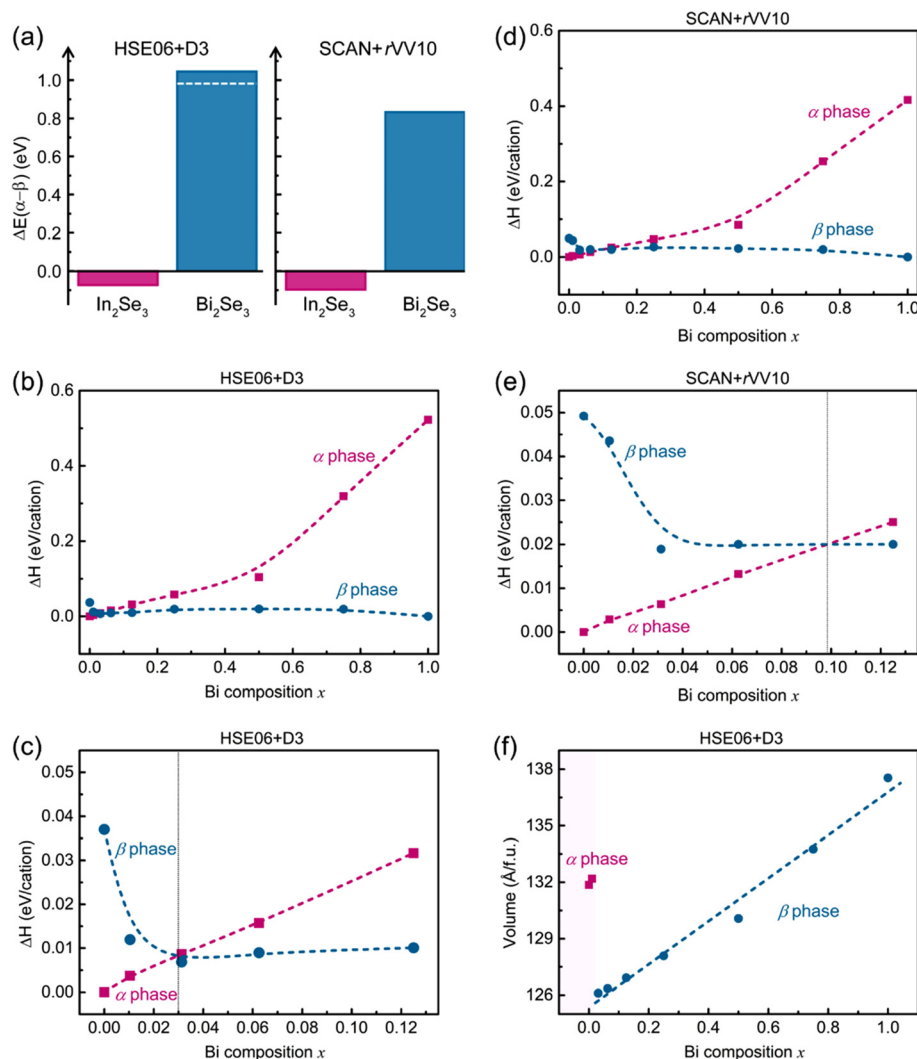


FIG. 2. Energy difference per formula unit (containing two cations) between the α and β phases of In_2Se_3 and Bi_2Se_3 calculated using HSE06+D3 and SCAN+rVV10. The calculated value for Bi_2Se_3 , including the effects of SOC, is indicated by the white dashed line. Mixing enthalpy per cation of $(\text{Bi}_x\text{In}_{1-x})_2\text{Se}_3$ alloys as a function of Bi content x in both α (purple-red squares) and β (blue circles) structures using (b) HSE06+D3 and (d) SCAN+rVV10. The enthalpies of pure α - In_2Se_3 and β - Bi_2Se_3 are both set to zero. Mixing enthalpy with an enlarged Bi composition scale of dilute $x=0$ –0.125 using (c) HSE06+D3 and (e) SCAN+rVV10. The vertical gray dotted lines represent the critical concentration x_c for the $\alpha \rightarrow \beta$ phase transition. (f) Volume per formula unit of $(\text{Bi}_x\text{In}_{1-x})_2\text{Se}_3$ alloys in the stable phase from HSE06+D3. The dashed lines are for guiding the eye.

smaller than that of $\sim 10\%$ using SCAN+rVV10. While the two functionals yield different quantitative results, they both qualitatively predict that the substitution of In by Bi at low concentrations stabilizes the β phase.

Figure 2(f) illustrates the calculated alloy volume per formula unit as a function of Bi content x for the $(\text{Bi}_x\text{In}_{1-x})_2\text{Se}_3$ alloy in the stable phase from HSE06+D3. Specifically, for $x = 0-0.3$, the volume of the α phase is shown with purple-red squares, while for $x = 0.3-1.0$, the volume of the β phase is shown with blue circles. It is evident that the alloy volume expands owing to the larger atomic size of Bi compared to In. For Bi compositions exceeding x_c , the volume of the alloy in the β phase exhibits a linear increasing trend with the concentration x , adhering to Vegard's law.³³

According to the Bragg-Williams approximation,³⁴ the mixing Gibbs free energy for the $(\text{Bi}_x\text{In}_{1-x})_2\text{Se}_3$ alloy can be written as a function of the Bi composition x and temperature T , as follows:

$$\Delta G(x, T) = \Delta H(x) - T\Delta S(x). \quad (3)$$

Here, the mixing enthalpy $\Delta H(x)$ can be described by a quadratic function based on the regular solution theory, i.e., $\Delta H(x) = \Omega x(1-x)$, where Ω is the interaction parameter. From the HSE06+D3 data shown in Fig. 3(b), the fitted interaction parameters are 0.68 and 0.095 meV for the α and β - $(\text{Bi}_x\text{In}_{1-x})_2\text{Se}_3$ alloys, respectively. $\Delta S(x)$ is the ideal configurational entropy of the random alloy, which can be written as $\Delta S(x) = -k_B[x\ln x + (1-x)\ln(1-x)]$, with k_B representing the Boltzmann constant. With the mixing Gibbs free energy, we construct the temperature-composition phase diagram for $(\text{Bi}_x\text{In}_{1-x})_2\text{Se}_3$ alloys with HSE06+D3, as shown in Fig. 3. The binodal (blue line) and spinodal (orange line) curves are determined by the conditions of $\partial G/\partial x = 0$ and $\partial^2 G/\partial x^2 = 0$, respectively. These curves, respectively, delineate the Gibbs free energy minimum and the boundary of alloys that are unstable at a given temperature.^{34,35}

The light orange region within the spinodal curve denotes the spinodal decomposition region, where spontaneous alloy decomposition may occur if sufficient atomic diffusion kinetics permit. In the temperature range above the binodal line, the alloy remains stable in either

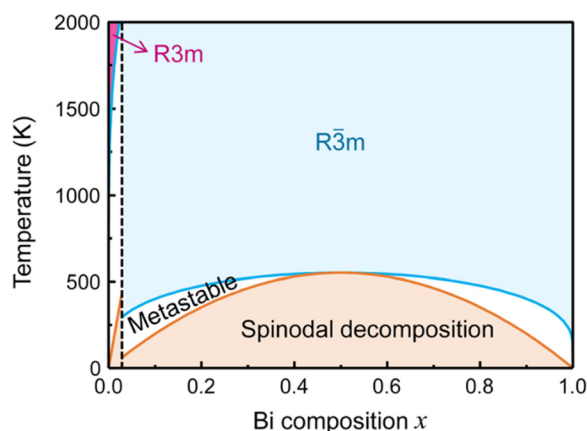


FIG. 3. Temperature-composition diagram with binodal (blue) and spinodal (orange) lines for $(\text{Bi}_x\text{In}_{1-x})_2\text{Se}_3$ alloys from HSE06+D3. The light orange and white regions represent the spinodal decomposition and metastable areas, respectively. The region above the binodal line indicates the stable phase in either the α or β phases.

the α or β phases. The area between the spinodal and binodal lines marks the metastable alloy phase (the white region). Beyond the critical Bi composition of $\sim 3\%$, the phase diagram of this heterostructural alloy $(\text{Bi}_x\text{In}_{1-x})_2\text{Se}_3$ closely resembles that of conventional isostructural phase systems, such as $\text{In}_{1-x}\text{Ga}_x\text{N}$.³⁴ The critical temperature $T_C = \Omega/2k_B$ for β - $(\text{Bi}_x\text{In}_{1-x})_2\text{Se}_3$ is estimated to be around 550 K, which is lower than its common experimental growth temperature of ~ 1000 K.^{16,36} This suggests that the formation of β - $(\text{Bi}_x\text{In}_{1-x})_2\text{Se}_3$ alloy by adding Bi into In_2Se_3 is feasible across the entire concentration range of $x > 3\%$.

The small critical Bi composition for the $\alpha \rightarrow \beta$ phase transition in $(\text{Bi}_x\text{In}_{1-x})_2\text{Se}_3$ alloys may be attributed to the strong preference of Bi atoms for octahedral sites over tetrahedral ones. Generally, ions with higher electronegativity and larger atomic radii tend to favor octahedral coordination. In and Bi atoms possess electronegativities of 1.73 and 1.92,³⁷ along with atomic radii of 1.42 and 1.51 Å,³⁸ respectively. As such, it can be inferred that Bi atoms exhibit a stronger preference for octahedral coordination compared to In atoms. Additionally, In^{3+} ion has an outer electronic configuration of $4d^{10}$ against $5d^{10}$ of Bi^{3+} ion. Therefore, Bi^{3+} ion favors octahedral coordination due to its less compressible nature. The preference of Bi for octahedral coordination with Se ligands is supported by the following computational findings:

- As stated above, β - Bi_2Se_3 with symmetry group $R\bar{3}m$ stands as the most stable form at ambient conditions, where all Bi atoms bond octahedrally to Se atoms. Notably, the energy difference between the α and β phases of Bi_2Se_3 surpasses that of In_2Se_3 significantly [see Fig. 2(a)]. Meanwhile, the relatively smaller difference observed from SCAN+rVV10 in comparison to HSE06+D3 comes with a relatively larger critical concentration for the $\alpha \rightarrow \beta$ phase transition in $(\text{Bi}_x\text{In}_{1-x})_2\text{Se}_3$ alloys.
- The coexistence of two different cation bonding environments in the α phase prompts inquiry into Bi's site preference upon its incorporation into α - In_2Se_3 . Our studies reveal a clear preference for sixfold coordinated sites by Bi, with a total energy difference of 0.92 eV per Bi between the two configurations.
- In alloys with $x \leq 50\%$, Bi occupies octahedral sites. However, as the Bi content exceeds 50%, Bi atoms have to incorporate into tetrahedral sites within the α phase. As shown in Fig. 2(b), the increasing slope of mixing enthalpy of α - $(\text{Bi}_x\text{In}_{1-x})_2\text{Se}_3$ alloy for x above 50% is steeper than that for x below 50%.

In conclusion, we have performed first-principles calculations, including the vdW interactions, to explore the phase stability and transition of the $(\text{Bi}_x\text{In}_{1-x})_2\text{Se}_3$ system across the entire range of Bi composition ($x = 0-1$). Results from both HSE06+D3 and SCAN+rVV10 calculations consistently show that, unlike Bi_2Se_3 , whose β phase exhibits significantly higher stability than the α phase, the formation enthalpy for α - In_2Se_3 is only marginally smaller than that of the β phase, shedding light on the ground-state inconsistency. Analysis of the composition-structure relationships and temperature-composition phase diagrams for $(\text{Bi}_x\text{In}_{1-x})_2\text{Se}_3$ alloys indicates that the substitution of In by Bi atoms at low concentrations stabilizes the β phase, consistent with previous experimental observations. Through a careful examination of computational findings and cation orbital nature, we demonstrate that the strong preference of Bi atoms for octahedral sites over tetrahedral ones underlies the observed small critical composition

for the $\alpha \rightarrow \beta$ phase transition. This study provides a fundamental understanding of the phase stability in $(\text{Bi}_x\text{In}_{1-x})_2\text{Se}_3$ alloys.

This work was supported by the National Natural Science Foundation of China (Grant Nos. 12204471 and 62304264), I.E. and A.J. acknowledge funding from the National Science Foundation (NSF) Award #OIA- 2217786.

AUTHOR DECLARATIONS

Conflict of Interest

The authors have no conflicts to disclose.

Author Contributions

Huachun Wang: Data curation (equal); Formal analysis (equal); Funding acquisition (equal); Investigation (equal); Methodology (equal); Validation (equal); Visualization (equal). **Xuefen Cai:** Conceptualization (equal); Data curation (equal); Funding acquisition (equal); Investigation (equal); Methodology (equal); Project administration (equal); Supervision (equal); Validation (equal); Visualization (equal); Writing – original draft (equal); Writing – review & editing (equal). **Wei Li:** Data curation (equal); Formal analysis (equal); Investigation (equal); Validation (equal); Visualization (equal). **Bin Wang:** Formal analysis (equal); Validation (equal); Visualization (equal). **Igor Evangelista:** Formal analysis (equal); Methodology (equal); Software (equal); Validation (equal); Visualization (equal). **Anderson Janotti:** Conceptualization (equal); Funding acquisition (equal); Investigation (equal); Methodology (equal); Project administration (equal); Resources (equal); Supervision (equal); Visualization (equal); Writing – original draft (equal); Writing – review & editing (equal).

DATA AVAILABILITY

The data that support the findings of this study are available from the corresponding authors upon reasonable request.

REFERENCES

- G. Almeida, S. Dogan, G. Bertoni, C. Giannini, R. Gaspari, S. Perissinotto, R. Krahne, S. Ghosh, and L. Manna, *J. Am. Chem. Soc.* **139**, 3005 (2017).
- S. Chen, X. Liu, X. Qiao, X. Wan, K. Shehzad, X. Zhang, Y. Xu, and X. Fan, *Small* **13**, 1604033 (2017).
- R. B. Jacobs-Gedrim, M. Shanmugam, N. Jain, C. A. Durcan, M. T. Murphy, T. M. Murray, R. J. Matyi, R. L. Moore, and B. Yu, *ACS Nano* **8**, 514 (2014).
- Y.-R. Chang, P.-H. Ho, C.-Y. Wen, T.-P. Chen, S.-S. Li, J.-Y. Wang, M.-K. Li, C.-A. Tsai, R. Sankar, and W.-H. Wang, *ACS Photonics* **4**, 2930 (2017).
- G. Han, Z.-G. Chen, J. Drennan, and J. Zou, *Small* **10**, 2747 (2014).
- J. Cui, H. Peng, Z. Song, Z. Du, Y. Chao, and G. Chen, *Chem. Mater.* **29**, 7467 (2017).
- L. Yang, Z.-G. Chen, M. S. Dargusch, and J. Zou, *Adv. Energy Mater.* **8**, 1701797 (2018).
- T. Nian, Z. Wang, and B. Dong, *Appl. Phys. Lett.* **118**, 033103 (2021).
- C. Zheng, L. Yu, L. Zhu, J. L. Collins, D. Kim, Y. Lou, C. Xu, M. Li, Z. Wei, and Y. Zhang, *Sci. Adv.* **4**, eaar7720 (2018).
- W. Ding, J. Zhu, Z. Wang, Y. Gao, D. Xiao, Y. Gu, Z. Zhang, and W. Zhu, *Nat. Commun.* **8**, 14956 (2017).
- Y. Zhou, D. Wu, Y. Zhu, Y. Cho, Q. He, X. Yang, K. Herrera, Z. Chu, Y. Han, and M. C. Downer, *Nano Lett.* **17**, 5508 (2017).
- C. Cui, W.-J. Hu, X. Yan, C. Addiego, W. Gao, Y. Wang, Z. Wang, L. Li, Y. Cheng, and P. Li, *Nano Lett.* **18**, 1253 (2018).
- J. Y. Ye, S. S. Soeda, Y. N. Y. Nakamura, and O. N. O. Nittono, *Jpn. J. Appl. Phys.* **37**, 4264 (1998).
- M. Brahlek, N. Bansal, N. Koirala, S.-Y. Xu, M. Neupane, C. Liu, M. Z. Hasan, and S. Oh, *Phys. Rev. Lett.* **109**, 186403 (2012).
- J. Liu and D. Vanderbilt, *Phys. Rev. B* **88**, 224202 (2013).
- J. Sánchez-Barriga, I. Aguilera, L. V. Yashina, D. Y. Tsukanova, F. Freyse, A. N. Chaika, C. Callaert, A. M. Abakumov, J. Hadermann, A. Varykhalov, E. D. L. Rienks, G. Bihlmayer, S. Blügel, and O. Rader, *Phys. Rev. B* **98**, 235110 (2018).
- Z. Y. Wang, X. Guo, H. D. Li, T. L. Wong, N. Wang, and M. H. Xie, *Appl. Phys. Lett.* **99**, 023112 (2011).
- I. Levy, C. Youmans, T. A. Garcia, H. Deng, S. Alsheimer, C. Testelin, L. Krusin-Elbaum, P. Ghaemi, and M. C. Tamargo, *Nano Lett.* **20**, 3420 (2020).
- S. J. Rath, D. J. Smith, and J. Drucker, *Cryst. Growth Des.* **14**, 4617 (2014).
- H. Ji, A. Reijnders, T. Liang, L. M. Schoop, K. S. Burch, N. P. Ong, and R. J. Cava, *Mater. Res. Bull.* **48**, 2517 (2013).
- H. G. Bouanani, D. Eddike, B. Liautard, and G. Brun, *Mater. Res. Bull.* **31**, 177 (1996).
- J. Heyd, G. E. Scuseria, and M. Ernzerhof, *J. Chem. Phys.* **118**, 8207 (2003).
- S. Grimme, J. Antony, S. Ehrlich, and H. Krieg, *J. Chem. Phys.* **132**, 154104 (2010).
- S. Grimme, S. Ehrlich, and L. Goerigk, *J. Comput. Chem.* **32**, 1456 (2011).
- J.-H. Yang, J.-S. Park, J. Kang, W. Metzger, T. Barnes, and S.-H. Wei, *Phys. Rev. B* **90**, 245202 (2014).
- G. Kresse and D. Joubert, *Phys. Rev. B* **59**, 1758 (1999).
- G. Kresse and J. Furthmüller, *Phys. Rev. B* **54**, 11169 (1996).
- C. Chatillon, *J. Cryst. Growth* **129**, 297 (1993).
- S. Popović, A. Tonejc, B. Gržeta-Plenković, B. Čelustka, and R. Trojko, *J. Appl. Crystallogr.* **12**, 416 (1979).
- S. Park and B. Ryu, *J. Korean Phys. Soc.* **69**, 1683 (2016).
- C. Callaert, M. Bercx, D. Lamoen, and J. Hadermann, *Acta Crystallogr. B* **75**, 717 (2019).
- S. H. Wei, L. G. Ferreira, J. E. Bernard, and A. Zunger, *Phys. Rev. B* **42**, 9622 (1990).
- L. Vegard, *Z. Phys.* **5**, 17 (1921).
- I. Ho and G. B. Stringfellow, *Appl. Phys. Lett.* **69**, 2701 (1996).
- A. M. Holder, S. Siol, P. F. Ndione, H. Peng, A. M. Deml, B. E. Matthews, L. T. Schelhas, M. F. Toney, R. G. Gordon, and W. Tumas, *Sci. Adv.* **3**, e1700270 (2017).
- P. Lošťák, L. Beneš, S. Civiš, and H. Süßmann, *J. Mater. Sci.* **25**, 277 (1990).
- J. C. A. Boeyens, *Z. Naturforsch. B* **63**, 199 (2008).
- P. Pyykkö and M. Atsumi, *Chem. Eur. J.* **15**, 186 (2009).